

Article

Not peer-reviewed version

Exploring Time-Resolved Fluorescence Data: A Software Solution for Model Generation and Analysis

[Thomas-Otavio Peulen](#) *

Posted Date: 22 January 2025

doi: 10.20944/preprints202501.1615.v1

Keywords: time-resolved fluorescence; fluorescence lifetime imaging microscopy (FLIM); fluorescence correlation spectroscopy (FCS); Förster resonance energy transfer (FRET); software for fluorescence analysis; integrative modeling; time-correlated single photon counting (TCSPC)



Preprints.org is a free multidisciplinary platform providing preprint service that is dedicated to making early versions of research outputs permanently available and citable. Preprints posted at Preprints.org appear in Web of Science, Crossref, Google Scholar, Scilit, Europe PMC.

Copyright: This open access article is published under a Creative Commons CC BY 4.0 license, which permit the free download, distribution, and reuse, provided that the author and preprint are cited in any reuse.

Article

Exploring Time-Resolved Fluorescence Data: A Software Solution for Model Generation and Analysis

Thomas-Otavio Peulen^{1,2}

¹ Current address: Technical University Dortmund, Department of Chemistry and Chemical Biology, Physical Chemistry, Dortmund, Germany; thomas.peulen@tu-dortmund.de

² Rudolf Virchow Center for Integrative and Translational Bioimaging, University of Würzburg, Würzburg, Germany

Abstract: Time-resolved fluorescence techniques, such as fluorescence lifetime imaging microscopy (FLIM), fluorescence correlation spectroscopy (FCS), and time-resolved fluorescence spectroscopy, are ideally suited for investigating molecular dynamics and interactions in biological and chemical systems. However, the analysis and interpretation of these datasets require advanced computational tools capable of handling diverse models and datasets. This paper presents a comprehensive software solution designed for model generation and analysis of time-resolved fluorescence data. The software supports the integration of multiple fluorescence techniques and provides users with robust tools for performing complex model analysis across diverse experimental data. With its ability to facilitate such a global analysis, model generation, data visualization, and sampling over model parameters, the software enhances the interpretability of intricate fluorescence phenomena. By providing flexible modeling capabilities, this solution offers a versatile platform for researchers to extract meaningful insights from time-resolved fluorescence data, aiding in the understanding of dynamic molecular processes.

Keywords: time-resolved fluorescence; fluorescence lifetime imaging microscopy (FLIM); fluorescence correlation spectroscopy (FCS); Förster resonance energy transfer (FRET); software for fluorescence analysis; integrative modeling; time-correlated single photon counting (TCSPC)

1. Introduction

Time-resolved fluorescence techniques, such as fluorescence lifetime imaging microscopy (FLIM), fluorescence correlation spectroscopy (FCS), time-resolved fluorescence spectroscopy, Förster resonance energy transfer (FRET), and single-molecule FRET, have become indispensable tools in the study of molecular dynamics and interactions [1]. These techniques provide critical insights into biological and chemical systems by enabling the observation of processes at nanosecond to microsecond timescales [2]. Despite their immense potential, the interpretation of time-resolved fluorescence data remains a significant challenge due to the complexity and size of the datasets, as well as the need for specialized models to accurately describe the phenomena under investigation [3]. Such an accurate description is necessary for integrative modelling that relies on accurate distance information [4,5].

In response to these challenges, this paper introduces a comprehensive software solution tailored for the analysis of time-resolved fluorescence data. The software integrates advanced techniques and facilitates global modeling, parameter linking, and robust uncertainty estimation. For example, it has previously been used to analyze FRET and DEER data to resolve minor states in proteins through fluorescence decay analysis and uncertainty estimation of single FRET pairs [6]. It has also supported the analysis of networks of distances [7–11], and provided combined TCSPC and FCS analyses for error estimation in FRET networks [2]. Furthermore, it has enabled fluorescence

correlation spectroscopy (FCS) analysis in vitro [12,13] and in cellular environments, demonstrating its flexibility and applicability across a wide range of experimental systems [14].

The software integrates computational tools and supports multiple fluorescence techniques, offering researchers a robust and versatile platform for analyzing diverse experimental datasets. By facilitating global analysis, model generation, and data visualization, the software aims to enhance the interpretability of complex fluorescence phenomena and advance our understanding of dynamic molecular processes. In the software, parameters of models are treated as nodes in a graph. This approach allows the creation of complex models by combining simpler models, enabling users to construct sophisticated frameworks for analyzing intricate fluorescence data. By linking and integrating different models, researchers can address multifaceted experimental questions with greater precision and flexibility.

Fluorescence measurements are increasingly applied for quantitative studies of biomolecules, as they allow us to investigate large, complex biomolecular systems in solution and even in live cells. Time-resolved fluorescence techniques provide a wealth of information about molecular environments, interactions, and dynamics. Comparative advantages of fluorescence experiments include the time resolution in the nanosecond range, which avoids structural averaging; the possibility to study single molecules, which allows us to resolve multiple states; and the ability to capture dynamics, which allows us to extract exchange pathways, equilibrium constants, and relaxation times. FRET measurements, where energy transfer between a donor (D) and an acceptor (A) probe can be employed to obtain inter-dye distances in multi-state systems, are increasingly used for integrative structure modeling of biomolecules and for revealing their kinetics [1,2,7,10,15–18]. Accurate FRET distances require reference samples (**Figure 1a**). Accurate time-resolved FRET experiments need donor reference samples [19] while intensity-based FRET experiments are calibrated using acceptor references (or directly excited acceptors in a FRET sample) [20]. Calibrated single-molecule FRET (smFRET) experiments give quantitative information on distances and molecular kinetics via single-molecule histograms (Figure 1b) [21–23]. In fluorescence correlation spectroscopy (FCS) single photon data is correlated. The fluctuations in fluorescence intensity inform on diffusion and molecular interactions (**Figure 1b**). FCS in living-cells can inform on binding [24] while FCS combined with fluorescence lifetime information gives information on intra-molecular kinetics [2,25,26].

Notably, FRET has the ability to resolve fast dynamic motions of more than 5 Å [18]. Crucial for quantitative FRET distances is the accurate treatment of statistical uncertainties and potential systematic uncertainties. The statistical uncertainties are mainly governed by the data noise (in single-photon counting shot-noise). Systematic uncertainties are related to calibration errors [20] and handling of the forward model (i.e., the model that computes for a given molecular structure experimental observables). Part of the forward model needs to consider orientational effects (κ^2) [27]. Uncertainties related to κ^2 can be reduced by considering the fluorescence anisotropy in the analysis workflow [28]. The general spectroscopic concepts valid in single-molecule spectroscopy can be directly applied to FLIM, for example, to map molecular interactions spatially in living systems [29–31].

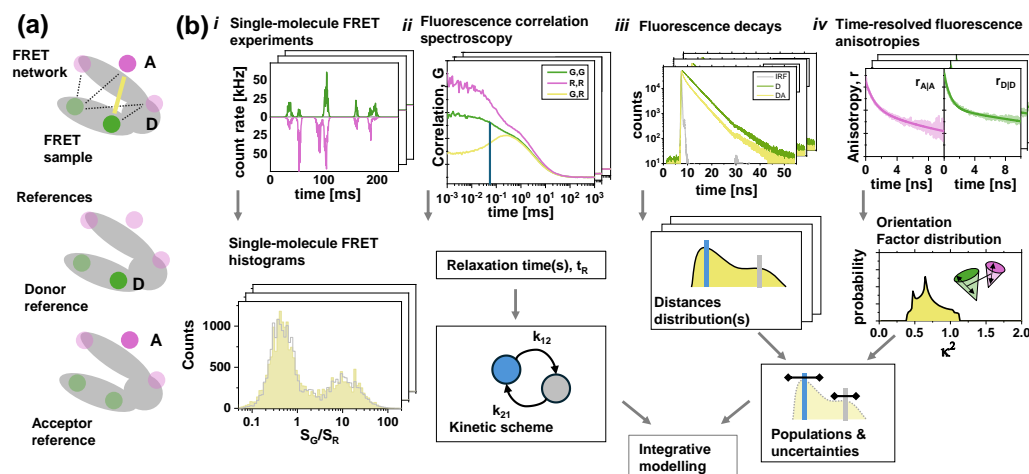


Figure 1. Samples, data types, and analysis workflow to recover kinetic and distance information for fluorescence based integrative modeling. (a) Data of multiple biomolecules (gray) fluorescent labeled by an acceptor (A, magenta) and a donor (D, green) are analyzed to obtain quantitative distance information for integrative FRET-based modeling. A set of FRET-labeled samples (FRET-network) is studied along with donor and acceptor references. (b) Time- and polarization-resolved single-molecule experiments using green (G) and red (R) detectors yield (i) single-molecule FRET histograms (S_G , green signal; S_R , red signal), (ii) auto- (G,G; R,R) and cross-correlation (G,R) fluorescence correlation spectroscopy (FCS) curves, (iii) fluorescence decay curves of the donor in the absence (D) and the presence of an acceptor (DA), and (iv) time-resolved fluorescence anisotropies. The experimental data is processed to obtain quantitative distance and kinetic information for integrative modelling. FRET efficiency histograms depend on kinetic schemes and distances, FCS provides relaxation times, t_R . Fluorescence decays provide distance distributions, time-resolved anisotropy informs on orientation factors.

Current tools for fluorescence data analysis often focus on specific techniques or lack the flexibility required for comprehensive analysis across multiple datasets [32–34]. This creates challenges for researchers seeking to integrate data from various fluorescence methods or apply custom models tailored to their experimental needs [35]. Addressing this gap requires software that supports diverse datasets, incorporates advanced algorithms, and provides intuitive interfaces for model creation and analysis. Some existing frameworks provide robust capabilities for analyzing imaging, single-molecule, and ensemble fluorescence data [32]. However, these tools often lack the ability to perform joint analyses by combining model parameters across different data types, such as FCS and TCSPC. As previously shown [22,36], a joint analysis is crucial for uncovering hidden states in biomolecular conformational dynamics. By combining fluorescence lifetimes and intensity-based FRET efficiency, such an approach proved to provide complementary insights into dynamics occurring on sub-millisecond timescales [35]. Analysis approaches to solve individual challenges exist. For instance, heterogeneous single-molecule histograms recover accurate distances and associated uncertainties for structural modeling by FRET [23,37,38]. However, there is a lack of an integrated approach that simplifies the interpretation of complex kinetic networks, offering a more comprehensive understanding of biomolecular behavior and function [22,36]. This highlights the need for integrated solutions that enable comprehensive and unified data analysis.

The proposed software solution offers a range of features designed to address the challenges of time-resolved fluorescence data analysis [19,23–25]. By supporting FLIM, FCS, and time-resolved fluorescence spectroscopy, the software enables researchers to analyze data from various experimental setups within a unified platform. Advanced computational tools are incorporated to provide robust solutions for fitting complex models and performing global analysis across multiple datasets. Users are also given the flexibility to define custom models and apply them to their data, enabling tailored analyses that address specific experimental questions. In addition to its modeling

capabilities, the software's user-friendly interface simplifies workflows, making it accessible to both novice and experienced researchers.

The software's versatility makes it suitable for a wide range of applications in biological and chemical research. For instance, it can be used to analyze fluorescence lifetimes and correlations, revealing details about molecular interactions such as binding events, conformational changes, and energy transfer processes [2,7,15,29,39–41]. Integrative modeling, including molecular models and dynamic structural biology, is another key application. Time-resolved fluorescence techniques can provide critical data for constructing molecular models, elucidating conformational changes, and understanding the kinetics of dynamic systems [22,36].

The Methods and Materials section details the software's implementation, including algorithms, frameworks, and supported data formats, and explains its handling of smFRET, FCS, photon distribution analysis, and FLIM data for versatile experimental workflows. The Results section highlights the software's capabilities through a comprehensive workflow that integrates smFRET, FCS, fluorescence decays, and time-resolved anisotropy, showcasing the importance of integrative modeling in understanding molecular interactions. A specific application example demonstrates the processing of synthetic smFRET data for a three-state system with kinetic exchange, along with FCS and TCSPC global analyses to validate the software's robustness and accuracy. Finally, the software's utility is illustrated by analyzing live-cell FLIM data, emphasizing its practical use in studying dynamic molecular processes in complex biological environments.

2. Materials and Methods

2.1. Software

ChiSurf was developed to jointly analyze multiple datasets and sample χ^2 surfaces and posterior model densities. It is implemented in Python with a graphical user interface designed using PyQt. The software organizes data and models into "fits," where models are equipped with parameters that can be defined as free, fixed, or linked. Linked parameters introduce dependencies between fits, enabling the grouping of individual fits into global fits. This feature allows for the analysis of complex, interconnected datasets. ChiSurf supports multiple experimental techniques, including time-correlated single-photon counting (TCSPC), fluorescence correlation spectroscopy (FCS), and single-molecule Förster resonance energy transfer (smFRET) efficiency histograms. It facilitates the combination of models from different experimental setups, allowing for comprehensive descriptions across varied experiment types. This capability is crucial for deriving meaningful insights from diverse datasets.

A flexible "adapter" system that allows parameters from one component of the model—such as rate constants in a transition rate matrix—to be linked to other components. For instance, the equilibrium population of each species can be computed from the transition rate matrix and then used as the species fraction in time-correlated single photon counting (TCSPC) experiments. Simultaneously, the eigenvalues of that same transition rate matrix define the relaxation times relevant for fluorescence correlation spectroscopy (FCS). By combining the analysis of FCS and TCSPC datasets under one unified framework, Chisurf can resolve components of the transition rate matrix more reliably than separate analyses would allow. This integrated approach ensures that both equilibrium and kinetic aspects of the system are consistently and accurately modeled, leading to more robust and comprehensive interpretations of molecular kinetics.

User interactions with the graphical user interface directly link to commands in an embedded iPython shell, providing users with flexible scripting capabilities in addition to Jupyter Notebooks that facilitate development workflows. The open-source source code and documentation is continuously updated, and freely available (<https://github.com/fluorescence-tools/chisurf>). The compiled version comes with a complete Conda distribution. In addition to its core functionalities—designing models, introducing parameter dependencies, and optimizing or sampling parameters for

various data types—ChiSurf ensures adaptability and robustness for advanced fluorescence data analysis.

2.2. Nomenclature

To demonstrate the software's capabilities, we process multiparameter fluorescence detection (MFD) single-molecule and MFD image spectroscopy data. MFD setups have polarization-resolved “green” and “red” detection channels for the donor and acceptor, respectively. MFD-PIE (Pulsed-Interleaved Excitation) uses two light sources, referred to as “green” and “red”, to excite the sample. This allows assessing in FRET experiments the donor and acceptor fluorescence separately [42]. Subscripts refer to the excitation and detection of fluorescence. The subscript ...|G refers to an excitation of the sample by a “green” light source and the subscript ...|R refers to an excitation of the sample by a “red” light source. The green detection channel is referred to be the subscript G|.... The red detection channel is referred to by the subscript R|.... The subscript “R|G” refers to red detection given a green excitation. Molecular species are referred to by superscripts. The superscript (DA) refers to a molecular species with a donor and an acceptor. The superscript (D0) refers to a species without an acceptor fluorophore. We distinguish the detected signal, S , from the background, B , and the fluorescence intensity, I :

$$S = I + B \quad (1)$$

Moreover, we distinguish fluorescence intensities uncorrected spectral crosstalk and crosstalk corrected fluorescence intensities. Fluorescence intensities corrected for crosstalk are referred to by the “dye”. In a FRET experiment on species (i), $I_{D|D}^{(i)}$ and $I_{A|D}^{(i)}$ refer to the fluorescence intensity of the donor and the FRET sensitized acceptor, respectively. $I_{D|D}^{(i)}$ and $I_{A|D}^{(i)}$ can be computed using components, α_{ij} , of the crosstalk matrix, α , and components, $g_{X|Y}$, of the instrumental sensitivity matrix, g :

$$\begin{aligned} I_{D|D}^{(i)} &= g_{D|G}^{-1}(I_{G|G}^{(i)} - \alpha_{G|R}I_{R|G}^{(i)}) \\ I_{A|D}^{(i)} &= g_{A|R}^{-1}(I_{R|G}^{(i)} - \alpha_{R|G}I_{G|G}^{(i)}). \end{aligned} \quad (2)$$

The component α_{ij} of the crosstalk matrix is defined by the spectral properties of the fluorophore and experimental setup. The component $g_{X|Y}$ of the crosstalk matrix is an instrumental parameter for detecting the dye X by the detector Y . For instance, $g_{D|G}$ and $g_{A|R}$ are the sensitivities for detecting a donor and acceptor dye by the green and red detector, respectively [19]. In most FRET experiments, crosstalk from A to D, $\alpha_{G|R}F_{G|R}^{(i)}$, is small. Hence, crosstalk corrections of donor signals are often omitted, while corrections are often assumed to be identical for all conformational states [20,28,43,44].

In addition to the spectral features, the fluorescence quantum yield, Φ_X , of the fluorophore X needs to be considered to yield a fully corrected fluorescence intensity, $F_{X|...}$. For the species (i) the fluorescence intensity of the FRET sensitized acceptor corrected for the fluorescence quantum yield is

$$F_{A|D}^{(i)} = I_{A|D}^{(i)} / \Phi_A. \quad (3)$$

Note, in single molecule experiments the excitation irradiance is usually high. Thus, the quantum yields may be lower due to populated dark states, e.g. due to cis/trans isomerization in Cy5 [45], and may require additional corrections [42,46]. Additionally, distinct species can have distinct fluorescence quantum yields. Correcting experimental data often introduces additional complexity to the noise. Therefore, in the software, corrections are implemented as model perturbations.

2.2. Förster Theory

Our software provides generic models to describe the dipolar coupling between donor, D, and acceptor, A, fluorophores to measure distances via FRET. The efficiency of the energy transfer process

from D to A can be quantified by the corrected fluorescence intensities of D in the presence of A, $F_{D|D}^{(DA)}$, and the FRET sensitized acceptor fluorescence, $F_{A|D}^{(DA)}$, the change of the donor fluorescence in absence, $F_{D|D}^{(D0)}$, and presence of an acceptor, $F_{A|D}^{(DA)}$, or by changes of the fluorescence lifetime and relates to, k_{RET} , the rate constants of the FRET process:

$$E = \frac{F_{A|D}^{(DA)}}{F_{D|D}^{(DA)} + F_{A|D}^{(DA)}} = \frac{F_{D|D}^{(D0)} - F_{A|D}^{(DA)}}{F_{D|D}^{(D0)}} = \frac{\tau_{D0} - \tau_{DA}}{\tau_{D0}} = \frac{k_{RET}}{k_D + k_{RET}}. \quad (4)$$

The rate constant is k_D related to the donor radiative lifetime, τ_{D0} , ($k_D = 1/\tau_{D0}$) while the FRET rate constant, k_{RET} , depends on the inter-dye distance, R_{DA} . This dependence is quantitatively described by the Förster relationship,

$$k_{RET} = \frac{3}{2} \cdot \kappa^2 \cdot k_D \cdot \left(\frac{R_{0,r}}{R_{DA}} \right)^6. \quad (5)$$

Here, κ^2 is an orientation factor, dependent on the mutual fluorophore dipole orientation, and $R_{0,r}$ is the reduced dye pair Förster radius given by the refractive index, n , and the spectral overlap integral, J [47,48].

$$R_{0,r} = 9780 \cdot [J(\lambda) \cdot n^{-4}]^{\frac{1}{6}}. \quad (6)$$

We use the Förster relationship for simplifying analysis of FRET data when studying molecular interactions. Often the orientation factor κ^2 is assumed to be 2/3 (isotropic averaging). However, for freely rotating dyes it is time dependent [49]. Models that recover distances assuming 2/3 (without further evidence) recover apparent distances, R_{app} . The software implements different approaches for handling κ^2 described in more detail below (2.8 **Orientation factor distributions**).

2.3. Time-Resolved Experiments

Theoretical Background

Our software supports FRET analysis of time-resolved fluorescence decays to resolve distances and sample heterogeneities. The simplest case being an analysis of fluorescence decays in the absence and the presence FRET. Generally, time-resolved FRET measurements require no instrumental intensity calibration. They measure the excited state lifetime of the donor in the presence of FRET, $\tau_{DA}^{(i)} = (k_D + k_{RET}^{(i)})^{-1}$. Briefly, FRET rate constants are obtained by a global description of the donor fluorescence decay in the absence, $f_{D|D}^{(D0)}$, and in the presence, $f_{D|D}^{(DA)}$, of FRET:

$$\begin{aligned} f_{D|D}^{(D0)} &= e^{-k_D \cdot t} \\ f_{D|D}^{(DA)} &= e^{-k_D \cdot t} \cdot e^{-k_{RET} \cdot t} \\ f_{A|D}^{(AD)} &= \frac{k_{RET}}{k_A - k_D - k_{RET}} \cdot (e^{-k_D \cdot t} \cdot e^{-k_{RET} \cdot t} - e^{-k_A \cdot t}) \end{aligned} \quad (7)$$

Here, $f_{D|D}^{(DA)}$ can be factorized into $\epsilon_D(t)$, the time-dependent depopulation of the donor (FRET induced donor decay), and $f_{D|D}^{(D0)}$. Such factorizing showed to be also accurate for multi-exponential $f_{D|D}^{(D0)}$ if FRET and other quenching processes are uncorrelated [19]. The FRET-induced donor decay depends on R_{DA} and κ^2 :

$$\epsilon_D(t) = \int \int p(\kappa^2, R_{DA}, t) e^{-t \cdot \frac{3}{2} \kappa^2 \cdot \frac{1}{\tau_{F,D}} \left(\frac{R_{0,r}}{R_{DA}} \right)^6} dR_{DA} d\kappa^2. \quad (8)$$

Above, $p(\kappa^2, R_{DA}, t)$ is a time-dependent distribution. It is difficult to disentangle $p(\kappa^2, R_{DA}, t)$ to obtain a distance distribution, $p(R_{DA})$. Four common approximations help determining $p(R_{DA})$: (i) κ^2 and R_{DA} are independent; (ii) $p(\kappa^2)$ is known (often assumed isotropic); (iii) dipoles are assumed to either rotate very fast slow to eliminate the κ^2 time-dependence. (iv) a reduced set of parameters is used to describe $p(R_{DA})$, e.g., the mean and variance of normal distribution.

For independent κ^2 and R_{DA} :

$$p(\kappa^2, R_{DA}) = p(\kappa^2) \cdot p(R_{DA}) \quad (9)$$

When molecular simulations are used to sample the orientation factor distribution in a sterically confined space, a simulated orientation factor distribution can be used for $p(\kappa^2)$ [50]. Alternatively, $p(\kappa^2)$ can be simulated based on experimental anisotropies e.g. using the diffusion in a cone model. Both approaches are implemented in our analysis software. For fast rotating dipoles (small fluorophores) compared to k_{RET} , the orientation factor distribution is approximated by an average $\langle \kappa^2 \rangle$.

$$\epsilon_{D, \kappa_{dyn}^2}(t) = \int p(R_{DA}) e^{-t \cdot \frac{3}{2} \langle \kappa^2 \rangle \cdot \frac{1}{\tau_{F,D}} \left(\frac{R_{0,r}}{R_{DA}} \right)^6} dR_{DA} \quad (10)$$

Dipoles that rotate slow compared to k_{RET} are (for instance fluorescent proteins (FPs) better described by a static $p(\kappa^2)$:

$$\epsilon_{D, \kappa_{static}^2}(t) = \int \int p(\kappa^2) p(R_{DA}) e^{-t \cdot \frac{3}{2} \kappa^2 \cdot \frac{1}{\tau_{F,D}} \left(\frac{R_{0,r}}{R_{DA}} \right)^6} dR_{DA} d\kappa^2 \quad (11)$$

The rotational correlation time of FPs (~16 ns) is slow compared to their fluorescence lifetime (~2.6 ns) [51]. Intermediate cases can be modelled using simulations [49]. Similar considerations regarding the averaging regimes apply to the inter-dye distance. For small organic fluorophores, we recovered correct distance distributions using a static orientation model, even though there is considerable displacement of the dyes on the time-scale of FRET [19].

Inter-dye distributions, $p(R_{DA})$, can be approximate by a linear combination of normal distributions

$$p(R_{DA}; w_{DA}, \overline{R_{DA}}) = \frac{1}{2\pi\sigma_{DA}^2} e^{-\frac{1}{2} \left(\frac{R_{DA} - \overline{R_{DA}}}{\sigma_{DA}} \right)^2} \quad (12)$$

where w_{DA} and $\overline{R_{DA}}$ are the width and the center of the inter-dye distance distribution, respectively. Alternatively, $p(R_{DA})$ is described by a linear combination of chi distributions:

$$p(R_{DA}; \sigma_{dye}, R_{cc}) = \frac{R_{DA}}{R_{cc}} \cdot (N(R_{DA} | \sigma_{dye}, R_{cc}) - N(R_{DA} | \sigma_{dye}, -R_{cc})) \quad (13)$$

Here, σ_{dye} is the width of the spatial dye distribution, and R_{cc} is the center-to-center distance between the two dyes. Such description is accurate for flexible tethered dyes [29,39] but also applies to fluorescent proteins coupled via unstructured and flexible amino acids at the N- and C-termini [29,38].

Experimental nuisances, e.g., convolutions with the instrument response function, IRF, the background, and the anisotropy of the dyes, need to be considered to recover $p(R_{DA})$ parameters. Our software allows for a joint analysis of $f_{G|G}^{(D0)}(t)$ and $f_{G|G}^{(DA)}(t)$, the FRET-sensitized acceptor decay $f_{R|G}^{(DA)}(t)$, and the acceptor directly excited by a “red” light source, $f_{R|R}^{(DA)}(t)$. In DA, D0, and A0 species mixtures the registered fluorescence decay $f_{G|G}^{(mix)}$ is a species fraction and an excitation and detection probabilities-weighted combination of $f_{D|D}^{(DA)}$, $f_{D|G}^{(D0)}$, $f_{A|G}^{(DA)}$, and $f_{A|A}^{(A0)}$.

Time-Resolved Anisotropy

Fluorescence generally leads to signal depolarization. The extent of this effect is described by a property called anisotropy. Molecular motions on the timescale of the fluorescence lifetime affect the shape of the fluorescence intensity decays unless detection is done under magic angle conditions. By measuring the parallel and perpendicularly polarized component of the fluorescence decay $f_{||}(t)$ and $f_{\perp}(t)$

$$f_{||}(t) = \frac{1}{3} \cdot f(t) \cdot (1 + 2 \cdot G \cdot r(t)) \quad (14)$$

$$f_{\perp}(t) = \frac{1}{3} \cdot f(t) \cdot (1 - r(t))$$

the anisotropy decay $r(t)$ can be determined. Above, G is an experimental factor correcting for the relative sensitivity of the parallel / perpendicular detector. Note, in a microscope with a high numerical aperture, NA, an additional correction for mixing of parallel and perpendicular light is needed [52,53]. Both layers of corrections are implemented in our software.

A typical decay of anisotropy is modeled as a multi-exponential function such as:

$$r(t) = \sum_k b_i^{(k)} \exp\left(-\frac{t}{\rho^{(k)}}\right) \quad (15)$$

where $r_0 = \sum_k b_i^{(k)}$ is the fundamental anisotropy of the molecule. Being dependent on the fluorescence lifetime, the anisotropy r can also be used as indicator for FRET and for quantitative FRET measurements [54]. Besides rotational motions and lifetime changes, fluorescence depolarization can also be caused by energy transfer between chemically identical fluorophores. Homotransfer is also described by Förster's theory, i.e., dependence of transfer efficiency on the distance, but does not change the observed intensity decays, thus making anisotropy the only observable for this process. HomoFRET is commonly used to study protein interactions in situ by polarization microscopy [55–57], having the advantage of relative simplicity of labeling (one type of dye) and instrumentation (only polarization or polarization and frequency-domain FLIM). HeteroFRET has advantage of more observables, i.e., donor/acceptor intensity ratios, fluorescence lifetime, providing better distance resolution and options for controlling experiment conditions.

Implementation

To recover precise distances, our software includes comprehensive models for analyzing $f_{D|D}^{(DA)}$, $f_{D|G}^{(D0)}$, $f_{A|G}^{(DA)}$, and $f_{A|A}^{(A0)}$, incorporating corrections for nuisance parameters such as scattered light, background noise, time-shifts, and FRET-inactive species. These nuisance parameters are essential for addressing experimental artifacts that can distort the data, ensuring accurate recovery of distance and rate parameters. For example, background noise and scattered light can introduce spurious signals, while time-shifts may cause discrepancies in decay measurements. Accounting for FRET-inactive species helps isolate signals from active donor-acceptor pairs, reducing bias and improving model accuracy. In addition to classic FRET models, the software implements the Partial Donor-Donor Energy Migration model (PDDEM) [58], which accounts for forward and backward energy transfer. Sampling across model parameters allows for error estimation, enabling reliable distance measurements and integrative modeling for structural determination. All routines and models are accessible interactively through the graphical user interface (GUI) or via scripting.

2.4. Burst Analysis

Theoretical Background

Our software can process data from single-molecule confocal experiments. In such experiments, single molecules are detected during their free diffusion through a confocal volume. The resulting photon bursts are selected from the recorded photon trace after separation of the background. This is accomplished by applying a threshold for the maximum inter-photon time and a minimum photon number within a burst (typically 30-160 photons) [59]. The burst duration is determined mainly by the experimental setup and the molecular dimensions. As the molecules are freely diffusing, a distribution of burst durations is observed, and the fluorescence observables are averaged according to the individual burst durations. Due to the low number of photons (60-500 photons per burst) detected per burst, it is not practical to apply complex models to describe the fluorescence intensity decays [60].

Implementation

To process such data, **ChiSurf** provides Jupyter notebooks for burst selection [59] and burst-wise fluorescence lifetime analysis using maximum likelihood estimation (MLE) algorithms [60], and anisotropy analysis [61]. For each burst, intensity-based parameters (e.g., green and red count rates for green and red excitation) and anisotropy-based parameters (e.g., the number of photons in parallel and perpendicular polarizations) are determined, allowing for the construction of multi-dimensional frequency histograms. Burst selection and sub-ensemble analyses are conducted using NDxplorer, a module of **ChiSurf** specifically designed for creating and analyzing n-dimensional single-molecule histograms and exporting burst selections as sub-ensembles.

2.5. Single Molecule Histograms

Theoretical Background

Single molecule histograms computed for the signal detected by two distinct detectors are widely used to analyze single-molecule traces and determine distances via FRET or anisotropy, particularly in confocal microscopy data. The simplest way of analyzing these histograms is by fitting a sum of normal distributions to recover the means of the underlying populations [62,63]. However, the fitted width of populations in traditional methods has no physical meaning and overlapping cannot resolved be accurately and minor states may be overlooked. Furthermore, without proper weighting of the residuals the fit quality cannot be judged. These complications were overcome by Photon Distribution Analysis (PDA) and related methods [23,38,64–67].

Our software focuses on analyzing confocal-derived FRET histograms by using PDA, an approach that accounts for shot noise and Poisson photon statistics to provide more accurate insights into FRET efficiencies, rate constants, and population fractions overcoming the limitations of traditional methods ensuring a precise representation of the underlying populations [44,64,68–70]. We have implemented a generic PDA framework that can be used to analyze both anisotropy and FRET data [38] that takes Poisson statistics of the photon distribution and broadening caused by shot noise into account.

PDA is accomplished by calculating the probability $P(S_G, S_R)$ to observe a certain combination of photons collected in the “green” (G) and “red” (R) detection channel given a certain time-window:

$$P(S_G, S_R) = \sum_{F_G+B_G=S_G; F_R+B_R=S_R} P(F)P(F_G, F_R|F)P(B_G)P(B_R). \quad (16)$$

The fluorescence intensity distribution, $P(F)$, can be obtained from the total signal intensity distribution $P(S)$, assuming that the background signals B_G and B_R are distributed according to Poisson distributions, $P(B_G)$ and $P(B_R)$, with known mean intensities B_G and B_R . The conditional probability $P(F_G, F_R|F)$ is the probability of observing a particular combination of green and red fluorescence photons, F_G and F_R , provided that the total number of registered fluorescence photons is F , and can be expressed as a binomial distribution [41]:

$$P(F_G, F_R|F) = \frac{F!}{F_G!(F-F_G)!} p_G^{F_G} (1-p_G)^{F-F_G}. \quad (17)$$

Here, p_G is the probability a detected photon is registered in the “Green” detection channel. In a FRET experiment, the probability p_G is unambiguously related to the FRET efficiency E :

$$p_G = \left(1 - \alpha_{R|G} + \gamma \cdot \frac{E}{1-E}\right)^{-1}. \quad (18)$$

where $\gamma = (\Phi_A g_{A|R})/(\Phi_D g_{D|G})$ and $\alpha_{R|G}$ is the crosstalk from G to R channel. Knowledge of $P(S_G, S_R)$ is sufficient to compute 1D histograms of any FRET-related parameter, which can be expressed as a function of S_G and S_R (e.g. signal ratio S_G/S_R or FRET efficiency E) [23]. Fitting such histograms obtained for a single species requires only one free parameter, p_G .

In PDA intensities are averaged on the millisecond timescale. Hence, the determined distances, R_E , are average distances and the distribution width carries limited information for fast dynamic systems. Moreover, a varying acceptor quantum yield $\Phi_{F,A}^{(A0)}$ results in broadening of the observed FRET distributions beyond the shot noise [68]. Thus, often complex model functions are necessary to

describe experimental data. In practice broadening associated to $\Phi_{F,A}^{(A0)}$ is well approximated by Gaussian distance distributions [71]. Additionally, in anisotropy experiments, the “green” and “red” detectors correspond to parallel and perpendicular detectors. Instead of p_G (relating FRET efficiency and photon detection probability in the green channel), the anisotropy model is used [23].

Implementation

To account for more complex cases, our software decouples PDA histogram computation of raw signals from derived parameters such as FRET efficiency and anisotropy. This modular framework enables flexible analysis of various experimental relations and setups, supporting global fits with customizable models based on distributions of p_G . By separating raw signal processing from parameter derivation, the software allows researchers to incorporate advanced models through Python scripting. Decorated Python functions facilitate the generation of parameter transforms, which convert PDA histograms into new or more complex representations. This flexibility allows users to build and implement sophisticated models tailored to specific experimental needs, fostering greater adaptability and precision in analysis.

2.6. Fluorescence Correlation Spectroscopy

Theoretical Background

Our software supports fluorescence correlation spectroscopy (FCS) [72–74]. FCS in combination with FRET (FRET-FCS) was developed as a powerful tool [75,76] to study fluctuations in the time evolution of a signal distance change. FRET-FCS allows for the analysis of FRET fluctuations covering a time range of nanoseconds to seconds. Hence, it is a perfect method to study conformational dynamics of biomolecules, complex formation, folding and catalysis [75–83]. Structural fluctuations are reflected by the correlation function, which in turn provides restraints on the number of conformational states. In this section we briefly describe the simplest case of FRET-FCS and discuss various experimental scenarios [26].

Briefly, the auto/cross-correlation of two correlation channels S_A and S_B is given by:

$$G_{A,B}(t_c) = 1 + \frac{\langle \delta S_A(t) \cdot \delta S_B(t + t_c) \rangle}{\langle S_A(t) \rangle \langle S_B(t) \rangle} \quad (19)$$

If S_A equals S_B the correlation function is called autocorrelation function (ACF), otherwise a cross-correlation function (CCF). ACFs and CCFs can be analyzed to inform on kinetics, the number of molecules and species populations [22,36]. If all species are of equal brightness, the amplitude at zero time of the autocorrelation function, $G(0)$, allows to determine the mean number of molecules N in the detection volume:

$$G(t_c = 0) = 1 + \frac{1}{N} \cdot G_{diff}(t_c) \quad (20)$$

For a 3-dimensional (3D) Gaussian shaped detection/illumination volume the normalized diffusion term, G_{diff} , is given by:

$$G_{diff}(t_c) = \left(1 + \frac{t_c}{t_{diff}}\right)^{-1} \cdot \left(1 + \left(\frac{\omega_0}{z_0}\right)^2 \cdot \frac{t_c}{t_{diff}}\right)^{-\frac{1}{2}} \quad (21)$$

whereas ω_0 and z_0 are shape parameters of the detection volume $w(x, y, z) = \exp(-2(x^2 + y^2)/\omega_0^2) \exp(-2z^2/z_0)$. $G_{diff}(t_c)$ allows for direct assessment of the diffusion constant D_{diff} . For 1-photon excitation the characteristic diffusion time $t_{diff} = \omega_0^2/(4D_{diff})$ relates to the diffusion coefficient D_{diff} .

In the simplest case of a two-state system, with different FRET levels and exchange rate constants k_{12} and k_{21} and comparable diffusion coefficients, in the sole presence of DA-molecules, in the

absence of bleaching ($G_{GR} = G_{RG}$) and dark states (e.g., triplet states), the ACFs and the CCF have a simple analytical solution:

$$\begin{aligned} G_{GG}(t_c) &= 1 + \frac{1}{N} \cdot G_{diff}(t_c) \cdot \left[1 + AC_{GG} \cdot \exp\left(-\frac{t_c}{t_R}\right) \right] \\ G_{RR}(t_c) &= 1 + \frac{1}{N} \cdot G_{diff}(t_c) \cdot \left[1 + AC_{RR} \cdot \exp\left(-\frac{t_c}{t_R}\right) \right] \\ G_{GR}(t_c) &= 1 + \frac{1}{N} \cdot G_{diff}(t_c) \cdot \left[1 - (AC_{GG} \cdot AC_{RR})^{1/2} \cdot \exp\left(-\frac{t_c}{t_R}\right) \right]. \end{aligned} \quad (22)$$

where AC_{GG} , AC_{RR} , and AC_{GR} are the amplitudes of the kinetic reaction terms and t_R is a relaxation time related to the exchange rate constants ($t_R = (k_{12} + k_{21})^{-1}$). The amplitudes depend on the molecular brightnesses, an intrinsic molecular property of the dyes and the FRET states [84]. The molecular brightness of species i is proportional to the product of the focal excitation irradiance, I_0 , the extinction coefficient, $\epsilon^{(i)}$, the fluorescence quantum yield, $\Phi_F^{(i)}$, and detection efficiencies $g_G^{(i)}$ or $g_R^{(i)}$ for green and red detectors for species i , respectively ($Q_{G,R}^{(i)} \propto I_0 \epsilon^{(i)} \Phi_F^{(i)} g_{G,R}^{(i)}$) [59,85]. The molecular brightness corresponds to the observed photon count rate per molecule, $Q^{(i)} = F^{(i)}/N^{(i)}$, where $F^{(i)}$ is the total number of fluorescence photons of $N^{(i)}$ molecules of species i . In the presence of FRET, efficiency $Q^{(i)}$ depends on the FRET efficiency, $E^{(i)}$, of the species i . The brightness and the FRET efficiencies are in practice often unknown. Hence, AC_{GG} , AC_{RR} , and AC_{GR} are treated as variable parameters.

Implementation

Our software provides Jupyter Notebooks for the computation of correlation functions allowing to implement advanced correlation techniques that increase the contrast. For example, fluorescence lifetime [86] can be utilized to distinguish molecular species based on their specific fluorescence lifetime, polarization, and spectral-resolved fluorescence decays [87]. The framework features a flexible "adapter" system, which allows parameters, such as rate constants in a transition rate matrix, to be linked to other model components, such as relaxation times. Such setup can be integrated within a theoretical framework for multi-state systems [22,36].

2.8. Orientation Factor Distributions

Theoretical Background

To determine accurate distances from FRET measurements we implemented methods for assessing κ^2 uncertainties, as κ^2 -error gathers most of the attention. For small dyes, the dye reorientation dynamics is on the timescale of FRET [58] and could be relevant for very short distances and dyes attached with short linkers [28,88,89]. For large fluorophores, e.g., fluorescent proteins, the fluorophore rotation is slow (≈ 16 ns) compared to the fluorescence lifetime (≈ 2.3 ns) [51]. Without molecular simulations the mutual fluorophore orientation is unknown. Thus, assuming an isotropic dipole orientation is reasonable. For isotropic oriented dipoles the orientation factor distribution is

$$p(\kappa^2) = \begin{cases} \frac{1}{2\sqrt{3}\kappa^2} \ln(2 + \sqrt{3}) & 0 \leq \kappa^2 \leq 1 \\ \frac{1}{2\sqrt{3}\kappa^2} \ln\left(\frac{2+\sqrt{3}}{\sqrt{\kappa^2+\sqrt{\kappa^2-1}}}\right) & 1 \leq \kappa^2 \leq 4 \end{cases}. \quad (23)$$

For a single DA distance, R_{DA} , a single FRET rate, k_{RET} , is observed if the fluorophores rotate fast compared to the fluorescence lifetime, $p(\kappa^2)$ can be replaced by its average $\langle \kappa^2 \rangle = 2/3$ (dynamic average). If the fluorophores rotate slow compared to the fluorescence lifetime, for a single R_{DA} a distribution of FRET rate constants, $p(k_{RET})$, will be observed (static average). In both cases, $p(k_{RET})$ can be computed using $p(\kappa^2)$.

For small fast rotating dyes, it has been demonstrated how to experimentally test whether the assumption for $\langle \kappa^2 \rangle \cong 2/3$ is justifiable or not [28]. For a given model of the fluorophores, e.g., the

“wobble in a cone” (WIC) model [88], it is possible to calculate a distribution of all possible values of κ^2 consistent with experimental data. In the WIC model κ^2 follows

$$\kappa^2 = \frac{2}{3} + \frac{2}{3} S_D^{(2)} S^{(2)}(\beta_1) + \frac{2}{3} S_A^{(2)} S^{(2)}(\beta_2) + \frac{2}{3} S_D^{(2)} S_A^{(2)} [S^{(2)}(\delta) + 6S^{(2)}(\beta_1)S^{(2)}(\beta_2) + 1 + 2S^{(2)}(\beta_1) + 2S^{(2)}(\beta_2) - 9\cos\beta_1\cos\beta_2\cos\delta] \quad (24)$$

where, β_1 and β_2 are the angles between the symmetry axes of the dye's rotations and the distance vector R_{DA} , while δ is the angle between the dye cone symmetry. A donor that is oriented approximately perpendicular to the linker axis is restricted to the half angle of a “disk”, $\theta_{disk} = \theta_D$. This is the case for fluorophore Alexa488. Alternatively, the dipole moment oriented along the linker axis can wobble with the opening half angle $\theta_{cone} = \theta_A$. This is approximately the case for Cy5 and Alexa647. For such geometry, the second-rank order parameters $S^{(2)}$ are:

$$\begin{aligned} S^{(2)}(\delta) &= \frac{1}{2}(3\cos^2\delta - 1), \\ S^{(2)}(\beta_1) &= \frac{1}{2}(3\cos^2\beta_1 - 1), \\ S^{(2)}(\beta_2) &= \frac{1}{2}(3\cos^2\beta_2 - 1), \\ S_D^{(2)} &= -\frac{1}{2}\cos^2\theta_{disk}, \text{ and} \\ S_A^{(2)} &= \frac{1}{2}\cos\theta_{cone}(1 + \cos\theta_{cone}). \end{aligned} \quad (25)$$

Only a subset of all dye orientations is possible for a certain combination of residual anisotropy of the donor, $r_{\infty,D|D}$, the direct excited acceptor, $r_{\infty,A|A}$, and the FRET-sensitized acceptor, $r_{\infty,A|D}^{(DA)}$. This restricts the possible angles between donor and acceptor motions and the second-rank order parameters $S^{(2)}$ relate to residual anisotropies as follows:

$$\begin{aligned} -S_D^{(2)} &= \sqrt{\frac{r_{\infty,D|D}}{r_0}}, \\ S_A^{(2)} &= \sqrt{\frac{r_{\infty,A|A}}{r_0}}, \text{ and} \\ S^{(2)}(\delta) &= \frac{1}{r_0} \frac{r_{\infty,A|D}^{(DA)}}{S_D^{(2)} S_A^{(2)}}. \end{aligned} \quad (26)$$

Thus, anisotropy decays provide useful information in determining local and global motions of the dyes. As only certain $p(\kappa^2)$ are consistent with the dye rotation model. Note that κ^2 does not explicitly depend on the cone opening half angles θ_D and θ_A and the assumption of dye reorientation within a cone/disk is not needed to obtain all possible values of κ^2 . However, axially symmetric transition dipole orientation distributions are usually a good estimation for κ^2 [88]. In most recent studies $\langle \kappa^2 \rangle$ values are $\sim 2/3$ justifying isotropic averaging of dipoles and showing that the common misconception of FRET as inaccurate is not well founded. However, one cannot neglect a specific effect of the microenvironment [90–92], especially if slow exchange is expected.

2.9. Simulation of Synthetic Data

In real experiments, fluorescence decays are inherently complex due to various factors such as donor-acceptor (DA) distance distributions, brightness variations caused by the confocal excitation profile, and experimental artifacts like the instrumental response function and detector dark counts. These complexities were reproduced in simulations of freely diffusing molecules to generate realistic photon traces. Detailed technical information is provided in [87]. As in actual single photon counting experiments, Poissonian statistics dictate the experimental noise and the resulting statistical errors in subsequent analyses. This test case aims to evaluate whether simulated data of typical experimental quality can accurately recover distance models and assess the limitations affecting their precision.

Here, we simulate a three-state system was implemented, consisting of putative states (C_1 , C_2 , C_3) undergoing linear exchange. Thus, in our simulations, with the transition rate matrix

$$\frac{d}{dt} \begin{bmatrix} x^{(1)} \\ x^{(2)} \\ x^{(3)} \end{bmatrix} = \begin{bmatrix} -(k_{21} + k_{31}) & k_{12} & k_{13} \\ k_{21} & -(k_{12} + k_{32}) & k_{23} \\ k_{31} & k_{32} & -(k_{13} + k_{23}) \end{bmatrix} \begin{bmatrix} x^{(1)} \\ x^{(2)} \\ x^{(3)} \end{bmatrix} \quad (27)$$

$k_{13} = 0$, $k_{31} = 0$. Brownian dynamics (BD) simulations were used to mimic the statistics of typical single-molecule FRET (smFRET) experiments over a 1.5-hour measurement period. In the simulations, the rate constants with a slow exchange between C_1 and C_2 ($k_{12} = 10 \text{ ms}^{-1}$, $k_{21} = 2 \text{ ms}^{-1}$) and a fast exchange between C_2 and C_3 ($k_{23} = 1 \text{ ms}^{-1}$, $k_{32} = 4 \text{ ms}^{-1}$) result in a fast relaxation time ($t_{R,1} = 0.0815 \text{ ms}$) and a slow ($t_{R,2} = 0.212 \text{ ms}$). Simulated experiments can be reproduced using the simulation software and the simulation setting are accessible through the ModelArchive (<https://www.modelarchive.org/doi/10.5452/ma-a2hbq>) and Zenodo (DOI: 10.5281/zenodo.14636405), respectively.

2.10. FLIM Experiments

2.10.1. Sample Preparation

Measurements were performed in MEF mGBP7 deficient cells stably transduced with eGFP-mGBP7 and mCh-mGBP3. Generation, culture conditions and characterization of the cell line is described in [29,93]. MEF cells were seeded in fully supplemented DMEM medium and grown until 70-80% confluence in Nunc™ LabTek™ II 8-well chambers (ThermoFisher). For live cell pulsed-interleaved excitation (PIE) MFIS-FRET measurements, the medium was changed to pre-warmed FluoroBrite™ DMEM (Gibco). Cells were kept at 37°C during the measurements.

2.10.2. PIE Measurement

PIE experiments were performed on a confocal laser-scanning microscope (FV1000 Olympus, Hamburg, Germany) equipped with a single photon counting electronics with picosecond time-resolution (HydraHarp 400, PicoQuant, Berlin, Germany). eGFP was excited at 488 nm with a polarized, pulsed 20 MHz diode laser (LDH-D-C-485, Pico-Quant, Berlin, Germany) using a power of 28 nW at the objective. mCherry was excited at 565 nm with a white light laser with a 20 MHz repetition rate (NKT) using a power of 175 nW at the objective. The emitted light was collected through the same objective and separated into perpendicular and parallel polarization. A narrow range of eGFPs emission spectrum (bandpass filter: HC520/35, AHF, Tübingen, Germany) was then detected by single photon avalanche detectors (PDM50-CTC, Micro Photon Devices, Bolzano, Italy). mCherry fluorescence was detected by hybrid detectors (HPMC-100-40, Becker&Hickl, Berlin, Germany, with custom designed cooling). The mCherry detection wavelength range was set by bandpass filters (HC 609/54, AHF). During acquisition, we took images from cells in a 1024x1024 pixel resolution. To measure a single cell, we chose a 256x256 pixel ROI and collected 400 frames per image with 4 μs dwell time [29,93].

3. Results

3.1. Software Overview

The software provides an easy-to-use platform for analyzing time-resolved fluorescence data, combining a graphical user interface (GUI) with an interactive programming shell (iPython). This setup allows users to perform actions in the GUI while automatically generating corresponding shell commands, making both interactive exploration and scripting straightforward (**Figure 2a**). For linear workflows, Jupyter Notebook support is included, simplifying tasks like burst-wise analysis of single-molecule data (Notebooks→Burst Search).

Additional tools such as NDxplorer enable visualization (Tools→NDxplorer) and analysis of multi-dimensional single-molecule data, and modules for fluorescence lifetime imaging microscopy (FLIM) data analysis (Tools→TTTR→TTTR CLSM) are also included. Basic utilities, like computing

orientation factors using fluorescence anisotropy data (Tools→Anisotropy→Kappa2 distribution), are provided to support common experimental needs. These features make the software accessible and practical for both routine and advanced analyses.

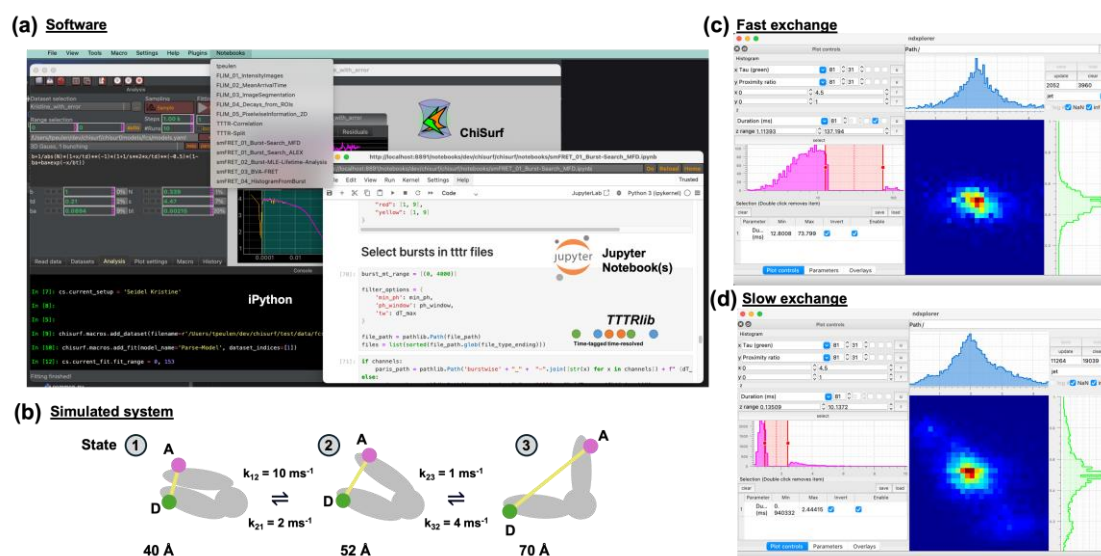


Figure 2. Synthetic 3-state system to demonstrate the single-molecule analysis workflow in ChiSurf. (a) Graphical user interface of ChiSurf, integrated Jupyter Notebook, and iPython environment. Single-molecule (sm) data can be processed either in ChiSurf (plugins) or via Jupyter Notebooks. Sm data is processed using ttrlib. (b) Simulated linear three state system. The exchange between state (1) and (2) is “fast”. The exchange between (2) and (3) is “slow”. In equilibrium, state (1), (2), and (3) have a population fraction of 13.8 %, 69 %, and 17.2%, respectively (Förster radius, $R_0 = 52 \text{ Å}$). (c) The in-built visualization tool for multiparametric single-molecule and FLIM data (NDXplorer; available via “Tools”) can be used to explore parameters and exported sub-ensemble data (e.g., bursts). The depicted histograms of the mean donor lifetime (“Tau (green)”) or the proximity ratio correspond to the synthetic system. (d) To visualize the states in the simulated smFRET experiments, exchange rate constants were scaled down by a factor of 10.

3.2. Simulated Test-System

To demonstrate the capabilities of the software, a simulated three-state system was generated to mimic typical single-molecule fluorescence experiments. This test system consists of three FRET states: high FRET (40 Å), mid FRET (52 Å), and low FRET (70 Å), with dynamic exchange occurring between the states. The system is representative of a protein with three conformational states (Figure 2b). Simulations were designed to emulate a typical single-molecule multiparameter fluorescence detection (smMFD) experiment, including polarization, color, and time-resolved fluorescence data.

The analysis workflow involves selecting photon bursts, performing maximum likelihood estimation (MLE) of fluorescence lifetimes, and analyzing anisotropy for each burst. For the system in fast exchange, only a single averaged population is observable due to the timescale of exchange being too rapid relative to the burst dwell time, resulting in averaged observables (Figure 2c). To ensure the robustness of the analysis and to visualize the distinct states in burst-wise data, the exchange rate constants were artificially slowed down by a factor of 10 in the simulations. Under these conditions, three distinct populations corresponding to the individual FRET states become visible, providing a clear demonstration of the software's ability to resolve and interpret dynamic systems.

The in-built visualization tool, NDXplorer, enhances the analysis by enabling users to explore multiparametric single-molecule data. It allows for selecting specific bursts (e.g. shown here in magenta/red) for downstream sub-ensemble analysis, providing a targeted approach for examining specific subsets of the data. For instance, histograms of the mean donor lifetime and proximity ratio illustrate the simulated system's behavior, validating the software's capacity to analyze complex

fluorescence dynamics (**Figure 2d**). This capability ensures that researchers can efficiently process and interpret data from dynamic systems with high precision.

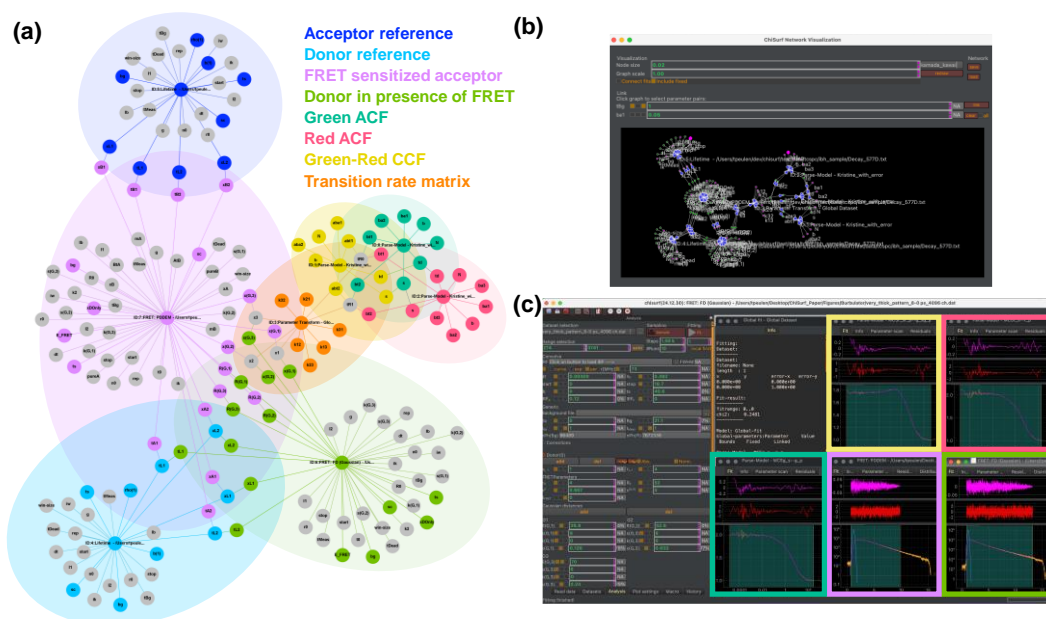


Figure 3. Global analysis of fluorescence correlation spectroscopy and fluorescence decay data. (a) Parameters of a global fluorescence decay and FCS analysis of a single FRET pair and associated reference samples. Parameters (circles with labels) emanate from models with associated datasets. Fixed and computed parameters are depicted as gray circles. The colors highlight the association of the fit parameters to datasets. Global analysis describes reference samples for fluorescence decays of the acceptor (dark blue, Acceptor reference) and the donor (light blue, Donor reference) in the absence of FRET, the fluorescence decay of the FRET sensitized acceptor emission (light magenta), the fluorescence decay of the donor in the presence of FRET (lime green), and fluorescence correlation spectroscopy (FCS) data. The global analysis describes FCS data of green (green, Green ACF) and red auto correlation functions (red, Red ACF) in addition to green/red cross-correlation functions (yellow, Green/Red CCF). Shared parameters across models of individual datasets are connected by lines. The colored ellipses in the background highlight the regions of individual models and parameter overlaps across models. The kinetic scheme (here 3-state kinetics) is the connecting element between the correlation curves and the fluorescence decays (orange, Transition rate matrix). (b) Visual representation of a parameter network in ChiSurf. (c) Graphical user interface and visualizing data and obtained model parameters.

3.3. Global Analysis

Global analysis has proven effective in resolving dynamic systems that are too fast for burst-wise single-molecule FRET analysis [22,36]. Fluorescence correlation spectroscopy (FCS) provides higher time resolution, revealing kinetic information such as relaxation times, while time-correlated single-photon counting (TCSPC) offers detailed distance, state, and population information. Here, we demonstrate a global analysis approach that combines FCS data—green/green autocorrelation (GG ACF), red/red autocorrelation (RR ACF), and green/red cross-correlation (GR CCF)—with TCSPC data, including fluorescence decays from donor-only references, directly excited acceptor references, donor fluorescence in the presence of FRET (yielding distance distributions), and FRET-sensitized acceptor fluorescence (**Figure 3a**).

This approach involves a substantial number of parameters. Each circle represents a parameter, with colored circles indicating variable parameters and connecting lines representing dependencies. Central circles correspond to individual datasets. Global analysis reduces the overall number of variable parameters by introducing dependencies across models. An adaptor, such as a transition rate matrix, is used to link FCS and TCSPC data by defining free parameters (e.g., rate constants) and

derived parameters (e.g., state populations and relaxation times). This integration enables both parameter optimization (fitting) and parameter sampling using Markov Chain Monte Carlo (MCMC) (**Figure 3a**) [94] as previously demonstrated [7].

Parameter dependencies can be introduced directly via the standard GUI, where each parameter includes an option to link, or through the “GlobalView” plugin, which provides a visual representation of the parameter network, datasets, and their dependencies (**Figure 3b**). An example analysis of a simulated “fast” three-state system demonstrates this approach, integrating GG ACF, RR ACF, GR CCF, FRET-sensitized emission, and donor fluorescence decay in the presence of FRET (**Figure 3c**). A global optimization recovers relaxation times of 0.022 ms and 0.176 ms, species amplitudes of 12.6%, 63.3%, and 24.0%, with corresponding distances of 39.8 Å, 52.6 Å, and 70.0 Å, respectively. This highlights the software’s ability to integrate diverse fluorescence datasets to extract detailed insights into dynamic molecular systems.

3.4. Fluorescence Lifetime Imaging

The software supports the processing of fluorescence lifetime imaging microscopy (FLIM) data across a variety of applications, with guanylate-binding proteins (GBPs) tethered to fluorescent proteins (FPs) serving as an illustrative example (**Figure 4a**). Integration with other software libraries is enabled through scripting, allowing workflows to be managed efficiently in Jupyter Notebooks. For example, multiparameter fluorescence detection with pulsed interleaved excitation (MFD PIE) data can be analyzed to generate fluorescence intensity images, including directly excited donors (green channel, prompt), FRET-sensitized acceptors (red channel, prompt), and directly excited acceptors (red channel, delay) (**Figure 4a**). Processing MFD PIE image data provides fluorescence lifetime information and insights into sample heterogeneities (**Figure 4b**). Intensity data can be used to segment images into distinct regions, such as the cytoplasm, vesicle-like structures (VLS), and the nucleus (**Figure 4c**). Sub-ensemble information from these segmented regions can then be exported for detailed analysis, enabling the determination of distance distributions (**Figure 4c**).

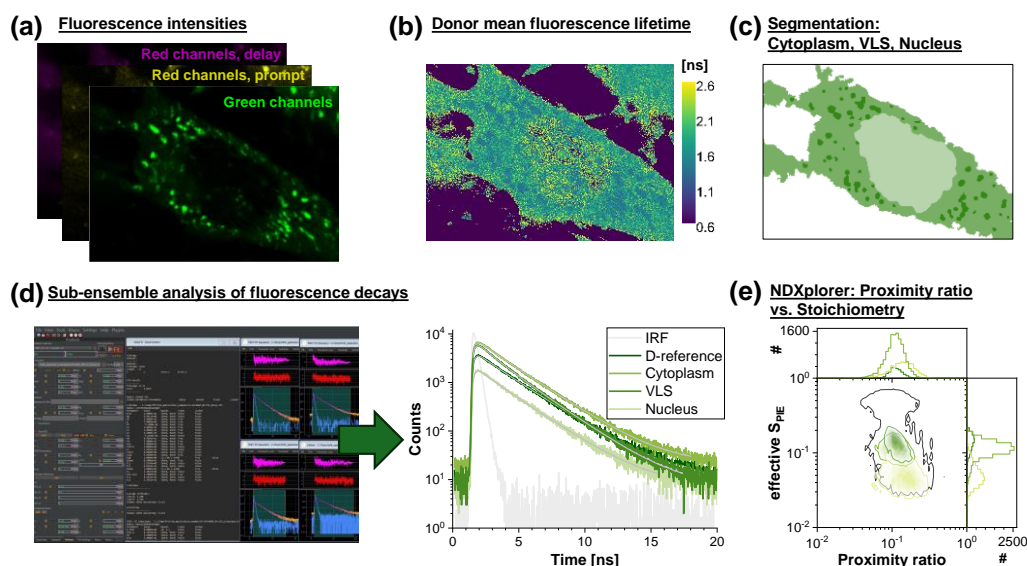


Figure 4. PIE-MFIS FLIM dataset of an MEF cell transfected with mGBP-eGFP and mGBP-mCherry. (a) Intensity images of the green (green), red prompt (yellow) and red delay (magenta) detection channels. The total intensity is calculated from the sum of the micro time events in the specified prompt and delay time windows as the sum over all acquired frames. (b) Mean donor photon arrival time calculated from the micro time distribution for the stacked frames. Only pixels with more than three detected photons per frame are considered. (c) Segmentation of intensity images into 3 pixel classes: cytoplasm (green), vesicle-like structures (VLS, dark green) and nucleus (light green). (d) Sub-ensemble analysis of the exported time-resolved fluorescence

intensities by jointly fitting with an appropriate donor reference. (e) Pixel-wise calculation of the apparent FRET efficiency and stoichiometry for each of the 3 pixel classes. Marginal projections of the parameter distributions are shown on the top and right, respectively.

The NDXplorer visualization tool further enhances analysis by enabling pixel-wise examination of spectroscopic features, allowing for a detailed understanding of spatial variations in fluorescence properties (**Figure 4d**). This robust and flexible workflow demonstrates the software's utility in analyzing FLIM data and its ability to provide detailed insights into biological and chemical systems.

4. Discussion

The presented software provides a powerful platform for the modeling of time-resolved fluorescence data, enabling the unification of diverse techniques such as FCS, TCSPC, smFRET, and FLIM. By linking parameters across datasets and applying shared models, it allows for comprehensive global analyses, reducing complexity and extracting detailed kinetic and structural insights. The example of a three-state system highlights its ability to integrate datasets and derive key parameters, demonstrating its value for studying dynamic molecular systems.

The inclusion of Bayesian modeling tools provides a rigorous framework for evaluating uncertainties and refining models, making it particularly suited for integrative structural biology. This approach ensures that data from various sources, from single-molecule experiments to measurements in living cells, can be combined to build cohesive models of molecular dynamics and interactions.

Looking ahead, the software offers potential for exporting graphical representations of systems and data, facilitating their integration into larger frameworks for molecular structure modeling. This capability would enable researchers to leverage diverse datasets in constructing dynamic structural models, bridging single-molecule observations with data acquired in complex biological environments. By supporting such integrative approaches, the software advances the understanding of molecular processes across scales and experimental contexts

Funding: The Bavarian State Ministry of Science and the Arts and the University of Würzburg supported TOP (Graduate School of Life Sciences, PostDocPlus).

Data Availability Statement: The software, input files, and example output files for the present work are available at <https://github.com/fluorescence-tools/chisurf>. No experimental data was generated as a part of this study. All experimental data used in this study was previously published and cited accordingly. Simulations used in this study are deposited in Zenodo (DOI: 10.5281/zenodo.14636405).

Acknowledgments: TOP thanks Katherina Hemmen for discussions and reading the manuscript. We thank Klaus Pfeffer and Daniel Degrandi for providing the cells with murine guanylate binding proteins 3 (mGBP3) and mGBP7.

Conflicts of Interest: The authors declare no conflicts of interest. The funders had no role in the design of the study; in the collection, analyses, or interpretation of data; in the writing of the manuscript; or in the decision to publish the results.

References

1. Lerner, E.; Barth, A.; Hendrix, J.; Ambrose, B.; Birkedal, V.; Blanchard, S.C.; Börner, R.; Sung Chung, H.; Cordes, T.; Craggs, T.D.; et al. FRET-Based Dynamic Structural Biology: Challenges, Perspectives and an Appeal for Open-Science Practices. *Elife* **2021**, *10*, doi:ARTN e60416 10.7554/eLife.60416.
2. Peulen, T.O.; Hengstenberg, C.S.; Biehl, R.; Dimura, M.; Lorenz, C.; Valeri, A.; Folz, J.; Hanke, C.A.; Ince, S.; Vöpel, T.; et al. Integrative Dynamic Structural Biology Unveils Conformers Essential for the Oligomerization of a Large GTPase. *Elife* **2023**, *12*, doi:10.7554/eLife.79565.

3. Hanke, C.A.; Westbrook, J.D.; Webb, B.M.; Peulen, T.O.; Lawson, C.L.; Šali, A.; Berman, H.M.; Seidel, C.A.M.; Vallat, B.K. Making Fluorescence-Based Integrative Structures and Associated Kinetic Information Accessible. *Nat. Methods* **2024**, 1–3, doi:10.1038/s41592-024-02428-x.
4. Dittrich, J.; Popara, M.; Kubiak, J.; Dimura, M.; Schepers, B.; Verma, N.; Schmitz, B.; Dollinger, P.; Kovacic, F.; Jaeger, K.-E.; et al. Resolution of Maximum Entropy Method-Derived Posterior Conformational Ensembles of a Flexible System Probed by FRET and Molecular Dynamics Simulations. *J. Chem. Theory Comput.* **2023**, 19, 2389–2409, doi:10.1021/acs.jctc.2c01090.
5. Russel, D.; Lasker, K.; Webb, B.; Velázquez-Muriel, J.; Tjioe, E.; Schneidman-Duhovny, D.; Peterson, B.; Sali, A. Putting the Pieces Together: Integrative Modeling Platform Software for Structure Determination of Macromolecular Assemblies. *PLoS Biol.* **2012**, 10, e1001244, doi:10.1371/journal.pbio.1001244.
6. Vöpel, T.; Hengstenberg, C.S.; Peulen, T.-O.; Ajaj, Y.; Seidel, C.A.M.; Herrmann, C.; Klare, J.P. Triphosphate Induced Dimerization of Human Guanylate Binding Protein 1 Involves Association of the C-Terminal Helices: A Joint Double Electron-Electron Resonance and FRET Study. *Biochemistry* **2014**, 53, 4590–4600, doi:10.1021/Bi500524u.
7. Sanabria, H.; Rodnin, D.; Hemmen, K.; Peulen, T.-O.; Felekyan, S.; Fleissner, M.R.; Dimura, M.; Koberling, F.; Kühnemuth, R.; Hubbell, W.; et al. Resolving Dynamics and Function of Transient States in Single Enzyme Molecules. *Nat. Commun.* **2020**, 11, 1231, doi:10.1038/s41467-020-14886-w.
8. Morales-Inostroza, L.; Folz, J.; Kühnemuth, R.; Felekyan, S.; Wieser, F.-F.; Seidel, C.A.M.; Göttinger, S.; Sandoghdar, V. An Optofluidic Antenna for Enhancing the Sensitivity of Single-Emitter Measurements. *Nat. Commun.* **2024**, 15, 2545, doi:10.1038/s41467-024-46730-w.
9. Imam, N.; Choudhury, S.; Hemmen, K.; Heinze, K.G.; Schindelin, H. Deciphering the Conformational Dynamics of Gephyrin-Mediated Collybistin Activation. *Biophys Rep (N Y)* **2022**, 2, 100079, doi:10.1016/j.bpr.2022.100079.
10. Hamilton, G.L.; Saikia, N.; Basak, S.; Welcome, F.S.; Wu, F.; Kubiak, J.; Zhang, C.; Hao, Y.; Seidel, C.A.M.; Ding, F.; et al. Fuzzy Supertertiary Interactions within PSD-95 Enable Ligand Binding. *Elife* **2022**, 11, e77242, doi:10.7554/eLife.77242.
11. Imam, N.; Choudhury, S.; Heinze, K.G.; Schindelin, H. Differential Modulation of Collybistin Conformational Dynamics by the Closely Related GTPases Cdc42 and TC10. *Front. Synaptic Neurosci.* **2022**, 14, 959875, doi:10.3389/fnsyn.2022.959875.
12. Tsytlonok, M.; Sanabria, H.; Wang, Y.; Felekyan, S.; Hemmen, K.; Phillips, A.H.; Yun, M.-K.; Waddell, M.B.; Park, C.-G.; Vaithiyalingam, S.; et al. Dynamic Anticipation by Cdk2/Cyclin A-Bound P27 Mediates Signal Integration in Cell Cycle Regulation. *Nat. Commun.* **2019**, 10, 1676, doi:10.1038/s41467-019-09446-w.
13. Tsytlonok, M.; Hemmen, K.; Hamilton, G.; Kolimi, N.; Felekyan, S.; Seidel, C.A.M.; Tompa, P.; Sanabria, H. Specific Conformational Dynamics and Expansion Underpin a Multi-Step Mechanism for Specific Binding of P27 with Cdk2/Cyclin A. *J. Mol. Biol.* **2020**, 432, 2998–3017, doi:10.1016/j.jmb.2020.02.010.
14. Hemmen^{1*}, K.; Choudhury^{1*}, S.; Friedrich, M.; Balkenhol, J.; Knöte, F.; Lohse, M.J.; Heinze, K.G. Dual-Color Fluorescence Cross-Correlation Spectroscopy to Study Protein-Protein Interaction and Protein Dynamics in Live Cells Available online: <https://app.jove.com/t/62954/dual-color-fluorescence-cross-correlation-spectroscopy-to-study> (accessed on 10 September 2024).
15. Hellenkamp, B.; Wortmann, P.; Kandzia, F.; Zacharias, M.; Hugel, T. Multidomain Structure and Correlated Dynamics Determined by Self-Consistent FRET Networks. *Nat. Methods* **2017**, 14, 174–180, doi:10.1038/nmeth.4081.
16. Dimura, M.; Peulen, T.-O.; Sanabria, H.; Rodnin, D.; Hemmen, K.; Hanke, C.A.; Seidel, C.A.M.; Gohlke, H. Automated and Optimally FRET-Assisted Structural Modeling. *Nat. Commun.* **2020**, 11, 5394, doi:10.1038/s41467-020-19023-1.
17. Chen, J.; Zaer, S.; Drori, P.; Zamel, J.; Joron, K.; Kalisman, N.; Lerner, E.; Dokholyan, N.V. The Structural Heterogeneity of α -Synuclein Is Governed by Several Distinct Subpopulations with Interconversion Times Slower than Milliseconds. *Structure* **2021**, 29, 1048–1064.e6, doi:10.1016/j.str.2021.05.002.
18. Agam, G.; Gebhardt, C.; Popara, M.; Mächtel, R.; Folz, J.; Ambrose, B.; Chamachi, N.; Chung, S.Y.; Craggs, T.D.; de Boer, M.; et al. Reliability and Accuracy of Single-Molecule FRET Studies for Characterization of

- Structural Dynamics and Distances in Proteins. *Nat. Methods* **2023**, *20*, 523–535, doi:10.1038/s41592-023-01807-0.
19. Peulen, T.O.; Opanasyuk, O.; Seidel, C.A.M. Combining Graphical and Analytical Methods with Molecular Simulations to Analyze Time-Resolved FRET Measurements of Labeled Macromolecules Accurately. *J. Phys. Chem. B* **2017**, *121*, 8211–8241, doi:10.1021/acs.jpcc.7b03441.
 20. Hellenkamp, B.; Schmid, S.; Doroshenko, O.; Opanasyuk, O.; Kühnemuth, R.; Rezaei Adariani, S.; Ambrose, B.; Aznauryan, M.; Barth, A.; Birkedal, V.; et al. Precision and Accuracy of Single-Molecule FRET Measurements-a Multi-Laboratory Benchmark Study. *Nat. Methods* **2018**, *15*, 669–676, doi:10.1038/s41592-018-0085-0.
 21. Gopich, I.V.; Szabo, A. FRET Efficiency Distributions of Multistate Single Molecules. *J. Phys. Chem. B* **2010**, *114*, 15221–15226, doi:10.1021/Jp105359z.
 22. Opanasyuk, O.; Barth, A.; Peulen, T.-O.; Felekyan, S.; Kalinin, S.; Sanabria, H.; Seidel, C.A.M. Unraveling Multi-State Molecular Dynamics in Single-Molecule FRET Experiments. II. Quantitative Analysis of Multi-State Kinetic Networks. *J. Chem. Phys.* **2022**, *157*, 031501, doi:10.1063/5.0095754.
 23. Kalinin, S.; Felekyan, S.; Antonik, M.; Seidel, C.A.M. Probability Distribution Analysis of Single-Molecule Fluorescence Anisotropy and Resonance Energy Transfer. *J. Phys. Chem. B* **2007**, *111*, 10253–10262, doi:10.1021/jp072293p.
 24. Kim, S.A.; Heinze, K.G.; Schwille, P. Fluorescence Correlation Spectroscopy in Living Cells. *Nat. Methods* **2007**, *4*, 963–973, doi:10.1038/nmeth1104.
 25. Gregor, I.; Enderlein, J. Time-Resolved Methods in Biophysics. 3. Fluorescence Lifetime Correlation Spectroscopy. *Photochem. Photobiol. Sci.* **2007**, *6*, 13–18, doi:10.1039/b610310c.
 26. Felekyan, S.; Sanabria, H.; Kalinin, S.; Kühnemuth, R.; Seidel, C.A.M. Analyzing Förster Resonance Energy Transfer with Fluctuation Algorithms. *Methods Enzymol.* **2013**, *519*, 39–85, doi:10.1016/B978-0-12-405539-1.00002-6.
 27. Dimura, M.; Peulen, T.O.; Hanke, C.A.; Prakash, A.; Gohlke, H.; Seidel, C.A. Quantitative FRET Studies and Integrative Modeling Unravel the Structure and Dynamics of Biomolecular Systems. *Curr. Opin. Struct. Biol.* **2016**, *40*, 163–185, doi:10.1016/j.sbi.2016.11.012.
 28. Sindbert, S.; Kalinin, S.; Nguyen, H.; Kienzler, A.; Clima, L.; Bannwarth, W.; Appel, B.; Müller, S.; Seidel, C.A.M. Accurate Distance Determination of Nucleic Acids via Förster Resonance Energy Transfer: Implications of Dye Linker Length and Rigidity. *J. Am. Chem. Soc.* **2011**, *133*, 2463–2480, doi:10.1021/ja105725e.
 29. Kravets, E.; Degrandi, D.; Ma, Q.; Peulen, T.-O.; Klümpers, V.; Felekyan, S.; Kühnemuth, R.; Weidtkamp-Peters, S.; Seidel, C.A.; Pfeffer, K. Guanylate Binding Proteins Directly Attack Toxoplasma Gondii via Supramolecular Complexes. *Elife* **2016**, *5*, doi:10.7554/eLife.11479.
 30. Somssich, M.; Ma, Q.; Weidtkamp-Peters, S.; Stahl, Y.; Felekyan, S.; Bleckmann, A.; Seidel, C.A.M.; Simon, R. Real-Time Dynamics of Peptide Ligand-Dependent Receptor Complex Formation in Planta. *Sci. Signal.* **2015**, *8*, ra76, doi:10.1126/scisignal.aab0598.
 31. Jares-Erijman, E.A.; Jovin, T.M. Imaging Molecular Interactions in Living Cells by FRET Microscopy. *Curr. Opin. Chem. Biol.* **2006**, *10*, 409–416, doi:10.1016/j.cbpa.2006.08.021.
 32. Schrimpf, W.; Barth, A.; Hendrix, J.; Lamb, D.C. PAM: A Framework for Integrated Analysis of Imaging, Single-Molecule, and Ensemble Fluorescence Data. *Biophys. J.* **2018**, *114*, 1518–1528, doi:10.1016/j.bpj.2018.02.035.
 33. Gao, D.; Barber, P.R.; Chacko, J.V.; Kader Sagar, M.A.; Rueden, C.T.; Grislis, A.R.; Hiner, M.C.; Eliceiri, K.W. FLIMJ: An Open-Source ImageJ Toolkit for Fluorescence Lifetime Image Data Analysis. *PLoS One* **2020**, *15*, e0238327, doi:10.1371/journal.pone.0238327.
 34. Globals Software Available online: <https://www.lfd.uci.edu/globals/> (accessed on 31 December 2024).
 35. Hancock, M.; Peulen, T.-O.; Webb, B.; Poon, B.; Fraser, J.S.; Adams, P.; Sali, A. Integration of Software Tools for Integrative Modeling of Biomolecular Systems. *J. Struct. Biol.* **2022**, *214*, 107841, doi:10.1016/j.jsb.2022.107841.

36. Barth, A.; Opanasyuk, O.; Peulen, T.-O.; Felekyan, S.; Kalinin, S.; Sanabria, H.; Seidel, C.A.M. Unraveling Multi-State Molecular Dynamics in Single-Molecule FRET Experiments. I. Theory of FRET-Lines. *J. Chem. Phys.* **2022**, *156*, 141501, doi:Artn 141501 10.1063/5.0089134.
37. Kalinin, S.; Peulen, T.; Sindbert, S.; Rothwell, P.J.; Berger, S.; Restle, T.; Goody, R.S.; Gohlke, H.; Seidel, C.A.M. A Toolkit and Benchmark Study for FRET-Restrained High-Precision Structural Modeling. *Nat. Methods* **2012**, *9*, 1218–1225, doi:10.1038/nmeth.2222 nmeth.2222 [pii].
38. Antonik, M.; Felekyan, S.; Gaiduk, A.; Seidel, C.A.M. Separating Structural Heterogeneities from Stochastic Variations in Fluorescence Resonance Energy Transfer Distributions via Photon Distribution Analysis. *J. Phys. Chem. B* **2006**, *110*, 6970–6978, doi:Doi 10.1021/Jp057257+.
39. Greife, A.; Felekyan, S.; Ma, Q.; Gertzen, C.G.W.; Spomer, L.; Dimura, M.; Peulen, T.O.; Wöhler, C.; Häussinger, D.; Gohlke, H.; et al. Structural Assemblies of the Di- and Oligomeric G-Protein Coupled Receptor TGR5 in Live Cells: An MFIS-FRET and Integrative Modelling Study. *Sci. Rep.* **2016**, *6*, 36792, doi:10.1038/srep36792.
40. Agam, G.; Barth, A.; Lamb, D.C. Folding Pathway of a Discontinuous Two-Domain Protein. *Nat. Commun.* **2024**, *15*, 690, doi:10.1038/s41467-024-44901-3.
41. Medina, E.; R Latham, D.; Sanabria, H. Unraveling Protein's Structural Dynamics: From Configurational Dynamics to Ensemble Switching Guides Functional Mesoscale Assemblies. *Curr. Opin. Struct. Biol.* **2021**, *66*, 129–138, doi:10.1016/j.sbi.2020.10.016.
42. Kudryavtsev, V.; Sikor, M.; Kalinin, S.; Mokranjac, D.; Seidel, C.A.M.; Lamb, D.C. Combining MFD and PIE for Accurate Single-Pair Forster Resonance Energy Transfer Measurements. *Chemphyschem* **2012**, *13*, 1060–1078, doi:10.1002/cphc.201100822.
43. Clegg, R.M. Fluorescence Resonance Energy Transfer and Nucleic Acids. *Methods Enzymol.* **1992**, *211*, 353–388, doi:10.1016/0076-6879(92)11020-j.
44. Sisamakias, E.; Valeri, A.; Kalinin, S.; Rothwell, P.J.; Seidel, C.A.M. Accurate Single-Molecule FRET Studies Using Multiparameter Fluorescence Detection. *Methods Enzymol.* **2010**, *475*, 455–514, doi:10.1016/S0076-6879(10)75018-7 S0076-6879(10)75018-7 [pii].
45. Widengren, J.; Schweinberger, E.; Berger, S.; Seidel, C.A.M. Two New Concepts to Measure Fluorescence Resonance Energy Transfer via Fluorescence Correlation Spectroscopy: Theory and Experimental Realizations. *J. Phys. Chem. A* **2001**, *105*, 6851–6866, doi:Doi 10.1021/Jp010301a.
46. Rothwell, P.J.; Berger, S.; Kensch, O.; Felekyan, S.; Antonik, M.; Wohrl, B.M.; Restle, T.; Goody, R.S.; Seidel, C.A.M. Multiparameter Single-Molecule Fluorescence Spectroscopy Reveals Heterogeneity of HIV-1 Reverse Transcriptase: Primer/Template Complexes. *Proc. Natl. Acad. Sci. U. S. A.* **2003**, *100*, 1655–1660, doi:10.1073/pnas.0434003100.
47. Förster, T. Experimentelle Und Theoretische Untersuchung Des Zwischenmolekularen Übergangs von Elektronenanregungsenergie. *Zeitschrift für Naturforschung* **1949**, *4*, 321–327.
48. Roberti, M.J.; Giordano, L.; Jovin, T.M.; Jares-Erijman, E.A. Corrigendum: FRET Imaging by Kt/Kf. *Chemphyschem* **2011**, *12*, 1033–1033, doi:10.1002/cphc.201190031.
49. Hummer, G.; Szabo, A. Dynamics of the Orientational Factor in Fluorescence Resonance Energy Transfer. *J. Phys. Chem. B* **2017**, *121*, 3331–3339, doi:10.1021/acs.jpcc.6b08345.
50. van der Meer, W.B.; van der Meer, D.M.; Vogel, S.S. Optimizing the Orientation Factor Kappa-Squared for More Accurate FRET Measurements. In *FRET - Förster Resonance Energy Transfer: From Theory to Applications*; Medintz, I., Hildebrandt, N., Eds.; Wiley-VCH Verlag: Weinheim, Germany, 2014.
51. Striker, G.; Subramaniam, V.; Seidel, C.A.M.; Volkmer, A. Photochromicity and Fluorescence Lifetimes of Green Fluorescent Protein. *J. Phys. Chem. B* **1999**, *103*, 8612–8617, doi:Doi 10.1021/Jp991425e.
52. Koshioka, M.; Sasaki, K.; Masuhara, H. Time-Dependent Fluorescence Depolarization Analysis in Three-Dimensional Microspectroscopy. *Appl. Spectrosc.* **1995**, *49*, 224–228, doi:10.1366/0003702953963652.
53. Erdelyi, M.; Simon, J.; Barnard, E.A.; Kaminski, C.F. Analyzing Receptor Assemblies in the Cell Membrane Using Fluorescence Anisotropy Imaging with TIRF Microscopy. *PLoS One* **2014**, *9*, e100526, doi:10.1371/journal.pone.0100526.

54. Gohlke, C.; Murchie, A.I.H.; Lilley, D.M.J.; Clegg, R.M. Kinking of DNA and RNA Helices by Bulged Nucleotides Observed by Fluorescence Resonance Energy-Transfer. *Proc. Natl. Acad. Sci. U. S. A.* **1994**, *91*, 11660–11664, doi:DOI 10.1073/pnas.91.24.11660.
55. Tramier, M.; Coppey-Moisán, M. Fluorescence Anisotropy Imaging Microscopy for Homo-FRET in Living Cells. *Methods Cell Biol.* **2008**, *85*, 395–414, doi:10.1016/S0091-679X(08)85017-0.
56. Bader, A.N.; Hoetzel, S.; Hofman, E.G.; Voortman, J.; Henegouwen, P.M.P.V.E.; van Meer, G.; Gerritsen, H.C. Homo-FRET Imaging as a Tool to Quantify Protein and Lipid Clustering. *Chemphyschem* **2011**, *12*, 475–483, doi:DOI 10.1002/cphc.201000801.
57. Nguyen, T.A.; Sarkar, P.; Veetil, J.V.; Koushik, S.V.; Vogel, S.S. Fluorescence Polarization and Fluctuation Analysis Monitors Subunit Proximity, Stoichiometry, and Protein Complex Hydrodynamics. *PLoS One* **2012**, *7*, e38209, doi:10.1371/journal.pone.0038209 PONE-D-12-06627 [pii].
58. Isaksson, M.; Häggblöf, P.; Håkansson, P.; Ny, T.; Johansson, L.B.-A. Extended Förster Theory for Determining Intraprotein Distances: 2. an Accurate Analysis of Fluorescence Depolarisation Experiments. *Phys. Chem. Chem. Phys.* **2007**, *9*, 3914–3922, doi:10.1039/b701591g.
59. Fries, J.R.; Brand, L.; Eggeling, C.; Köllner, M.; Seidel, C.A.M. Quantitative Identification of Different Single Molecules by Selective Time-Resolved Confocal Fluorescence Spectroscopy. *J. Phys. Chem. A* **1998**, *102*, 6601–6613, doi:Doi 10.1021/Jp980965t.
60. Maus, M.; Cotlet, M.; Hofkens, J.; Gensch, T.; De Schryver, F.C.; Schaffer, J.; Seidel, C.A.M. An Experimental Comparison of the Maximum Likelihood Estimation and Nonlinear Least-Squares Fluorescence Lifetime Analysis of Single Molecules. *Anal. Chem.* **2001**, *73*, 2078–2086, doi:10.1021/ac000877g.
61. Schaffer, J.; Volkmer, A.; Eggeling, C.; Subramaniam, V.; Striker, G.; Seidel, C.A.M. Identification of Single Molecules in Aqueous Solution by Time-Resolved Fluorescence Anisotropy. *J. Phys. Chem. A* **1999**, *103*, 331–336, doi:Doi 10.1021/Jp9833597.
62. Brünger, A.T.; Strop, P.; Vrljic, M.; Chu, S.; Weninger, K.R. Three-Dimensional Molecular Modeling with Single Molecule FRET. *J. Struct. Biol.* **2011**, *173*, 497–505, doi:10.1016/j.jsb.2010.09.004.
63. McCann, J.J.; Choi, U.B.; Zheng, L.; Weninger, K.; Bowen, M.E. Optimizing Methods to Recover Absolute FRET Efficiency from Immobilized Single Molecules. *Biophys. J.* **2010**, *99*, 961–970, doi:10.1016/j.bpj.2010.04.063.
64. Gopich, I.; Szabo, A. Theory of Photon Statistics in Single-Molecule Förster Resonance Energy Transfer. *J. Chem. Phys.* **2005**, *122*, 14707, doi:10.1063/1.1812746.
65. Nir, E.; Michalet, X.; Hamadani, K.M.; Laurence, T.A.; Neuhauser, D.; Kovchegov, Y.; Weiss, S. Shot-Noise Limited Single-Molecule FRET Histograms: Comparison between Theory and Experiments. *J. Phys. Chem. B* **2006**, *110*, 22103–22124, doi:Doi 10.1021/Jp063483n.
66. Kalinin, S.; Felekyan, S.; Valeri, A.; Seidel, C.A.M. Characterizing Multiple Molecular States in Single-Molecule Multiparameter Fluorescence Detection by Probability Distribution Analysis. *J. Phys. Chem. B* **2008**, *112*, 8361–8374, doi:Doi 10.1021/Jp711942q.
67. Tomov, T.E.; Tsukanov, R.; Masoud, R.; Liber, M.; Plavner, N.; Nir, E. Disentangling Subpopulations in Single-Molecule FRET and ALEX Experiments with Photon Distribution Analysis. *Biophys. J.* **2012**, *102*, 1163–1173, doi:10.1016/j.bpj.2011.11.4025.
68. Gopich, I.V.; Szabo, A. Single-Macromolecule Fluorescence Resonance Energy Transfer and Free-Energy Profiles. *J. Phys. Chem. B* **2003**, *107*, 5058–5063, doi:10.1021/jp027481o.
69. Zhang, K.; Yang, H. Photon-by-Photon Determination of Emission Bursts from Diffusing Single Chromophores. *Abstracts of Papers of the American Chemical Society* **2006**, *231*, 21930–21937, doi:Doi 10.1021/Jp0546047.
70. Nettels, D.; Gopich, I.V.; Hoffmann, A.; Schuler, B. Ultrafast Dynamics of Protein Collapse from Single-Molecule Photon Statistics. *Proc. Natl. Acad. Sci. U. S. A.* **2007**, *104*, 2655–2660, doi:10.1073/pnas.0611093104.
71. Kalinin, S.; Sisamakias, E.; Magennis, S.W.; Felekyan, S.; Seidel, C.A.M. On the Origin of Broadening of Single-Molecule FRET Efficiency Distributions beyond Shot Noise Limits. *J. Phys. Chem. B* **2010**, *114*, 6197–6206, doi:10.1021/jp100025v.

72. Elson, E.L. 40 Years of FCS: How It All Began. In *Fluorescence Fluctuation Spectroscopy*; Tetin, S.Y., Ed.; Methods in Enzymology; Elsevier Academic Press Inc: San Diego, 2013; Vol. 518, pp. 1–10 ISBN 9780123884220.
73. Elson, E.L.; Magde, D. Fluorescence Correlation Spectroscopy. I. Conceptual Basis and Theory. *Biopolymers: Original Research on* **1974**, *13*, 1–27, doi:10.1002/bip.1974.360130102.
74. Magde, D.; Elson, E.; Webb, W.W. Thermodynamic Fluctuations in a Reacting System---Measurement by Fluorescence Correlation Spectroscopy. *Phys. Rev. Lett.* **1972**, *29*, 705–708, doi:10.1103/PhysRevLett.29.705.
75. Slaughter, B.D.; Allen, M.W.; Unruh, J.R.; Bieber Urbauer, R.J.; Johnson, C.K. Single-Molecule Resonance Energy Transfer and Fluorescence Correlation Spectroscopy of Calmodulin in Solution. *J. Phys. Chem. B* **2004**, *108*, 10388–10397, doi:10.1021/jp040098u.
76. Torres, T.; Levitus, M. Measuring Conformational Dynamics: A New FCS-FRET Approach. *J. Phys. Chem. B* **2007**, *111*, 7392–7400, doi:10.1021/jp070659s.
77. Johnson, C.K. Calmodulin, Conformational States, and Calcium Signaling. A Single-Molecule Perspective. *Biochemistry* **2006**, *45*, 14233–14246, doi:10.1021/bi061058e.
78. Price, E.S.; Aleksiejew, M.; Johnson, C.K. FRET-FCS Detection of Intralobe Dynamics in Calmodulin. *J. Phys. Chem. B* **2011**, *115*, 9320–9326, doi:10.1021/jp203743m.
79. Price, E.S.; DeVore, M.S.; Johnson, C.K. Detecting Intramolecular Dynamics and Multiple Förster Resonance Energy Transfer States by Fluorescence Correlation Spectroscopy. *J. Phys. Chem. B* **2010**, *114*, 5895–5902, doi:10.1021/jp912125z.
80. Slaughter, B.D.; Unruh, J.R.; Allen, M.W.; Bieber Urbauer, R.J.; Johnson, C.K. Conformational Substates of Calmodulin Revealed by Single-Pair Fluorescence Resonance Energy Transfer: Influence of Solution Conditions and Oxidative Modification. *Biochemistry* **2005**, *44*, 3694–3707, doi:10.1021/bi048595o.
81. Gurunathan, K.; Levitus, M. FRET Fluctuation Spectroscopy of Diffusing Biopolymers: Contributions of Conformational Dynamics and Translational Diffusion. *J. Phys. Chem. B* **2010**, *114*, 980–986, doi:10.1021/jp907390n.
82. Levitus, M. Relaxation Kinetics by Fluorescence Correlation Spectroscopy: Determination of Kinetic Parameters in the Presence of Fluorescent Impurities. *J. Phys. Chem. Lett.* **2010**, *1*, 1346–1350, doi:10.1021/jz100231v.
83. Al-Soufi, W.; Reija, B.; Novo, M.; Felekyan, S.; Kühnemuth, R.; Seidel, C.A.M. Fluorescence Correlation Spectroscopy, a Tool to Investigate Supramolecular Dynamics: Inclusion Complexes of Pyronines with Cyclodextrin. *J. Am. Chem. Soc.* **2005**, *127*, 8775–8784, doi:10.1021/ja0508976.
84. Kim, S.A.; Heinze, K.G.; Bacia, K.; Waxham, M.N.; Schwille, P. Two-Photon Cross-Correlation Analysis of Intracellular Reactions with Variable Stoichiometry. *Biophys. J.* **2005**, *88*, 4319–4336, doi:10.1529/biophysj.104.055319.
85. Eggeling, C.; Berger, S.; Brand, L.; Fries, J.R.; Schaffer, J.; Volkmer, A.; Seidel, C.A.M. Data Registration and Selective Single-Molecule Analysis Using Multi-Parameter Fluorescence Detection. *J. Biotechnol.* **2001**, *86*, 163–180, doi:10.1016/S0168-1656(00)00412-0.
86. Böhmer, M.; Wahl, M.; Rahn, H.-J.; Erdmann, R.; Enderlein, J. Time-Resolved Fluorescence Correlation Spectroscopy. *Chem. Phys. Lett.* **2002**, *353*, 439–445, doi:10.1016/S0009-2614(02)00044-1.
87. Felekyan, S.; Kalinin, S.; Sanabria, H.; Valeri, A.; Seidel, C.A.M. Filtered FCS: Species Auto- and Cross-Correlation Functions Highlight Binding and Dynamics in Biomolecules. *Chemphyschem* **2012**, *13*, 1036–1053, doi:10.1002/cphc.201100897.
88. Dale, R.E.; Eisinger, J.; Blumberg, W.E. Orientational Freedom of Molecular Probes - Orientation Factor in Intra-Molecular Energy-Transfer. *Biophys. J.* **1979**, *26*, 161–193, doi:10.1016/S0006-3495(79)85243-1.
89. Johansson, L.B.-A.; Edman, P.; Westlund, P.O. Energy Migration and Rotational Motion within Bichromophoric Molecules .2. A Derivation of the Fluorescence Anisotropy. *J. Chem. Phys.* **1996**, *105*, 10896–10904.
90. Dolgih, E.; Ortiz, W.; Kim, S.; Krueger, B.P.; Krause, J.L.; Roitberg, A.E. Theoretical Studies of Short Polyproline Systems: Recalibration of a Molecular Ruler. *J. Phys. Chem. A* **2009**, *113*, 4639–4646, doi:10.1021/jp811395r.

91. Dolgih, E.; Roitberg, A.E.; Krause, J.L. Fluorescence Resonance Energy Transfer in Dye-Labeled DNA. *Journal of Photochemistry and Photobiology A-Chemistry* **2007**, *190*, 321–327, doi:10.1016/j.jphotochem.2006.11.009.
92. VanBeek, D.B.; Zwier, M.C.; Shorb, J.M.; Krueger, B.P. Fretting about FRET: Correlation between Kappa and R. *Abstracts of Papers of the American Chemical Society* **2007**, *233*, 4168–4178, doi:DOI 10.1529/biophysj.106.092650.
93. Steffens, N.; Beuter-Gunia, C.; Kravets, E.; Reich, A.; Legewie, L.; Pfeffer, K.; Degrandi, D. Essential Role of MGBP7 for Survival of Toxoplasma Gondii Infection. *MBio* **2020**, *11*, doi:10.1128/mBio.02993-19.
94. Foreman-Mackey, D.; Hogg, D.W.; Lang, D.; Goodman, J. Emcee: The MCMC Hammer. *Publ. Astro. Soc. Pac.* **2013**, *125*, 306–312, doi:Doi 10.1086/670067.

Disclaimer/Publisher's Note: The statements, opinions and data contained in all publications are solely those of the individual author(s) and contributor(s) and not of MDPI and/or the editor(s). MDPI and/or the editor(s) disclaim responsibility for any injury to people or property resulting from any ideas, methods, instructions or products referred to in the content.